Research Square

Preprints are preliminary reports that have not undergone peer review.
They should not be considered conclusive, used to inform clinical practice,
or referenced by the media as validated information.

FCRLB-mediated dual control of tumor metabolism and macrophage polarization promotes lung cancer malignancy

Nueraili Maihemuti

22318055@zju.edu.cn

Zhejiang University https://orcid.org/0009-0005-0544-0122

Yueli Shi

Zhejiang Chinese Medical University

Sujing Jiang

Wenzhou Medical University

Pan Liu

Chinese Academy of Sciences

Zhen Shi

Fourth Military Medical University: Air Force Medical University

Zhiyong Xu

Zhejiang Cancer Hospital https://orcid.org/0000-0001-9873-8617

Research Article

Keywords: None-small cell lung cancer, Immunotherapy, Machine learning, multi-omics

Posted Date: October 31st, 2025

DOI: https://doi.org/10.21203/rs.3.rs-7784814/v1

License: This work is licensed under a Creative Commons Attribution 4.0 International License.
Read Full License

Version of Record: A version of this preprint was published at Journal of Translational Medicine on February 16th, 2026. See the published version at https://doi.org/10.1186/s12967-026-07872-1.

Abstract

Background

Anti–PD-1 therapy has improved outcomes in non-small cell lung cancer (NSCLC), yet primary and acquired resistance remain common. Pinpointing regulators of tumor–immune crosstalk is therefore critical to enhance therapeutic efficacy.

Methods

We integrated multi-omics sequencing with ensemble machine-learning to nominate prognostic genes in NSCLC, followed by pathway and intercellular-signaling analyses (pseudotime analysis, GSVA, and functional enrichment). We generated shRNA-mediated FCRLB-knockdown NSCLC cell lines and performed molecular and immunological assays. A murine lung-cancer xenograft model was used to validate the role of the candidate gene in tumor progression and its impact on the tumor microenvironment (TME).

Results

We identified FCRLB as a key gene influencing lung cancer prognosis via transcriptomic gene screening, and elucidated its unique roles in tumor cells and macrophages. FCRLB-highly expressing tumor cells exhibited high activation of the PI3K signaling and reactive oxygen species (ROS) pathways, regulated metabolic pathways such as pyridine metabolism and terpenoid quinone biosynthesis, and induced C-C motif chemokine ligand 2 (CCL2) production. Additionally, high FCRLB expression in monocyte-derived macrophages (mo-Macs) promoted M2-like polarization, thereby further exacerbating lung cancer malignancy.

Conclusions

Our data identify and functionally validate FCRLB as a pro-tumor regulator in NSCLC.FCRLB regulates the secretion of multiple cytokines (including CCL2) by tumor cells via the ROS pathway and PI3K signaling pathway, thereby promoting M2 polarization of macrophages. Additionally, FCRLB exerts a positive regulatory effect on the malignant progression of NSCLC. This finding provides a potential novel target for overcoming immunotherapys resistance in NSCLC.

1. Introduction

Lung cancer is well-recognized for its high incidence and mortality rates, imposing a substantial burden on public health. Surgical resection combined with chemotherapy remains the foundational treatment modality for non-small cell lung cancer (NSCLC) (1–3).Immunotherapies—such as anti-PD-1/PD-L1

agents have significantly enhanced the survival prognosis of NSCLC patients and ushered in revolutionary advances in NSCLC treatment(4, 5). However, the clinical efficacy of (6) is severely limited, with only about 20% of lung cancer patients responding to treatment. This low response rate is largely attributed to the immunosuppressive tumor microenvironment (TME), with tumor-associated macrophages (TAMs) being a major contributor. As the most abundant immune cell population in the TME, monocyte-derived macrophages (mo-Macs) are recruited by tumor-secreted cytokines such as CCL2 and CSF-1 and polarized in to pro- tumorigenesis M2 phenotypes. Crucially, they potently suppress the infiltration and function of cytotoxic T cells, promote distant metastasis, and are strongly correlated with poor clinical outcomes(7–9). And targeting the recruitment of mo-Macs is currently a critical strategy for improving the efficacy of immunotherapies(10, 11). Therefore, investigating how tumor cells drive immunotherapy resistance by modulating macrophages is crucial for developing new strategies to target macrophage recruitment and re-sensitize tumors to treatment.

Machine learning has been maturely utilized in the screening of prognostic targets for NSCLC. By assessing the strengths and limitations of multiple algorithms, implementing the optimal prognostic model construction strategy, and further evaluating target features via single-cell transcriptome sequencing or multi-omics integrative analysis, this approach can assist researchers in rapidly and accurately identifying key prognostic genes in tumors. For instance, a recent study integrated machine learning with single-cell transcriptomics to screen for key prognostic genes in lung adenocarcinoma (LUAD) cells, and subsequently analyzed these genes via functional validation assays(12–14). Machine learning enables researchers to screen for prognostic genes in a high-throughput manner, and the integration of multiple algorithms for constructing prognostic models with multi-omics sequencing further greatly improves the accuracy of such predictions—thus establishing it as a crucial approach in the research of the NSCLC immune landscape.

In this study, to identify key mediators of NSCLC progress and immunotherapy resistance, we integrated multi-omics data and machine learning, and identified Fc receptor-like B (FCRLB) as a critical prognostic gene in NSCLC. Single-cell analyses localized FCRLB expression and linked it to ROS/PI3K pathway activity. Further mechanistic investigations revealed that FCRLB$^+$ tumor cells, through ROS/PI3K and CCL2-mediated crosstalk, orchestrate a pro-tumorigenic TME by recruiting M2 macrophages, thereby nominating it as a promising therapeutic target for overcoming immunotherapy resistance.

2. Materials and methods

2.1 Ordinary transcriptome data availability

The regular transcriptome data was obtained from GSE101929, consisting of 32 patients and 34 healthy individuals. The lung adenocarcinoma data (541 tumors and 59 healthy individuals) and lung squamous cell carcinoma data (502 tumors and 51 healthy individuals) were obtained from the TCGA database. R package Limma is used for differential analysis, R package org.Hs.eg.db and clusterProfiler are used for GO and KEGG enrichment, R package randomForest is used for random forest screening with an

importance threshold of 0.0003, selected as important genes for subsequent Cox analysis, and R package glmnet, survivminer, and survival are used for Cox regression analysis.

2.2 Acquisition and processing of scRNA-seq data

Single-cell dataset is from GSE131907. The Seurat software package is used for preliminary analysis of single-cell data. The cell quality control steps have been completed. Data normalization and selection of highly variable genes (2000) were selected. The functions used for data conversion were NormalizeData, FindVariableFeatures and ScaleData in the Seurat package. The dimensionality reduction methods UMAP, UMAP and clustering algorithm Louvian were used later, all from Seurat. The FindAllMarkers function to calculate the differential genes between Cluster or cell types, with pvalue less than 0.05, log2FC greater than 0.25, and the expression ratio should be greater than 0.1. VlnPlot and FeaturePlot functions are used to localize the violin graph and feature map of genes. The dim parameter is 15 and the resolution is 1. Cell annotations are given in the original text. The FindMarkers function is used for differential analysis of single-cell data, the R package ggplot2 is used for data visualization, and the R package pheatmap is used for heat map drawing.

2.3 Single-cell GSVA analysis and Single-cell cell analysis

The GSVA software package is used for cell subpopulation GSVA analysis, and the pathway score gene set uses the HallMark gene set in msigDB and the KEGG gene set in C2. The subtype classification of cells was analyzed by the Seurat software package. The dimensionality reduction method UMAP, UMAP and clustering algorithm Louvian all came from Seurat. The dims parameter of tumor cell subtype classification was 15 and the resolution parameter was 0.001; the dims parameter of macrophage subtype classification was 15 and the resolution parameter was 0.01. The Nebulosa software package was used for gene colocalization analysis of macrophage subtypes. count (FCRLB) > 0 was defined as FCRLB + cells, and count (FCRLB) = 0 was defined as FCRLB-cell.

The Cellchat package is used for cell communication analysis of single-cell data. Single cell data of macrophages and tumor cell subpopulations were combined into single cell communication data. The Monocle2 package is used for quasi-timed analysis of single-cell data. Gene expression trend min_expr = 0.5, and the remaining parameters are default.

The IrGSEA package is used for single-cell gene set analysis of single-cell data, tumor cells, and macrophage cells for single-cell gene set analysis. IrGSEA 1.0 uses the AUCell, UCell, Singapore, and ssgsea algorithms to calculate Hallmark gene set scores, and the difference analysis is used to calculate the Wilcoxon rank sum test (*p < 0.05, **p < 0.01, ***p < 0.001, ****p < 0.001, ****p < 0.0001).

All data processing, statistical analysis and plotting were performed in R 4.3.3.

2.4 Metabolomics data acquisition and analysis

Metabolomic data were obtained from the literature(15). R package ggplot2 is used for data visualization. For visualization: Use the R package ggplot2 to generate metabolite abundance heatmaps,

based on the processed metabolome data. Use the pheatmap package to draw a dual-index heatmap: Dual index: Row index (metabolite clustering) + column index. Blue-white-red tricolor mapping for standardized abundance values; row-wise clustering via Euclidean distance combined with Ward.D2 method.

2.5 Construction of FCRLB NSCLC knockdown cell line

Select two human lung cancer cell lines, NCI-H226 (Pricella, CL-0396) and NCI-H1975 (Pricella, CL-0298), and murine NSCLC cell line LLC (Pricella, CL-0140), and culture them in a cell culture incubator with RPMI-1640 medium supplemented with 10% fetal bovine serum and 1% penicillin/streptamycin. Construct a short hairpin RNA (shRNA) lentiviral vector (YouBio) containing a specific sequence (Table 1) and package the lentivirus. Following lentivirus infection for 24 hours, the medium was replaced, and successfully infected cells were selected using puromycin (Solarbio, P8230). Knockdown efficiency was assessed using qRT-PCR analysis.

2.6 RNA extraction and qRT-PCR

The RNA extraction process was performed using an RNA rapid extraction kit (RN001, Shanghai Yishan Biotechnology) following the manufacturer's protocols. Total RNA was reverse transcribed into cDNA using HiScript III all-in-one RT SuperMix Perfect for qPCR (R333-01, Vazyme). The qRT-PCR was conducted using ChamQ Universal SYBR qPCR Master Mix (Q711-02) in a CFX96 Touch Real Time PCR Detection System (BIO-RAD). Fluorescence data was collected at the end of each extension step. The specificity of the amplification products was verified by melting curve analysis, and primer sequences are listed in Table 1.

2.7 Western blot (WB) assay

Cells and tissues with similar density and well condition was added RIPA lysis buffer (Beyotime, P0013C) mixed with PMSF and phosphorylase inhibitor, thoroughly lyse on ice, sonicate the cells, centrifuge, and 5x DualColor Protein Loading Buffer (HANGZHOU FUDE BIOLOGICAL TECHNOLOGY, FD006) was added to the supernatant. Separate the protein using 10% SDS-PAGE and transfer the membrane. After blocking, the following primary antibodies: FCRLB (Proteintech, 17157-1-AP), β-actin (Cell Signaling, 4967S), p-PI3K (Cell Signaling,17366), p-AKT (Cell Signaling, 13038S), mTOR (Cell Signaling, 2972S) were used to incubate the membrane overnight. And the next day applied Anti rabbit IgG, Incubate HRP linked Antibody (Cell Signaling, 7074S) for one hour. The ChemiDoc™ Touch Imaging System (BIO-RAD) is used for chemiluminescence imaging scanning.

2.8 Construction of xenograft model in mice

Expand shctrl-LLC cells and shFCRLB-LLC cells in good condition. Obtain 6-week-old healthy male C57BL/6 mice from GemPharmatech company. Digest, centrifuge, and resuspend two types of LLC cells, adjusting the cell concentration to 1×107/mL. Subcutaneous inject 100 μL of cell suspension into the abdomen of mice using a syringe. Waiting for 7 days until a visible tumor grows, and then measure the tumor volume and mass every other day. Sacrifice mice after 21 days. After isolating the tumor tissue,

we subjected it to paraffin embedding and sectioning, followed by immunohistochemical (IHC) staining to detect the expression levels of CD86, CD206, and CCL2. This animal study was reviewed and approved by the Animal Experiment Ethics Committee of Zhejiang University before implementation (ZJU20250631).

2.9 FCRLB knockout NSCLC cell line proliferation ability test

After knocking out the FCRLB gene in the cell line, alteration in cell proliferation ability were detected using Cell Counting Kit-8 (CCK8) (Beyotime, C0038) reagent. After digestion and centrifugation of the cells, use the complete medium for resuspension. After counting, adjust the cell concentration to 3×10^4/mL. Add 100 μ L cells into the 96 well plate. After 0 h, 24 h, 48 h and 72 h of cell adhesion, add 10 μ LCCK8 reagent to incubate for 2 h. Then use the microplate reader (Tecan) to collect the absorbance of the sample at 450 nm wavelength.

2.10 Wound healing assay

H1975 and H226 cells (stably transfected with shCtrl or shFCRLB) in an appropriate growth state were seeded in 6-well plates and incubated overnight. The seeding density was adjusted to ensure the cells formed a confluent monolayer covering the entire well surface by the next day. Vertical lines were drawn on the bottom of each well with a marker pen, and several observation points were marked along each line. A sterile pipette tip was used to gently scratch the confluent cell monolayer along the pre-drawn vertical lines, and images of cells adjacent to the observation points were captured under a microscope. After subsequent incubation in serum-free medium for 24 h, images were captured again at the same positions. The scratch area was quantified using ImageJ software.

2.11 Transwell migration and invasion assay of NSCLC cells

The migration assay involves digesting and centrifuging the processed NSCLC cells, then resuspending them in a serum-free medium containing 0.5% BSA. The resuspended cells are then counted and adjusted to a concentration of 2×10^5/mL. 200μL of the cell suspension is added to the upper chamber of an 8μm transwell chamber (Corning,3422), and the chamber is then transferred to a 24-well plate containing complete medium for 24 hours of culture. The chamber is collected, washed three times, fixed with 4% PFA (Beyotime, P0099) at room temperature for 20 minutes, and stained with crystal violet staining solution (Beyotime, C0121) for 1 hour. The cells above the filter membrane are gently wiped off with a cotton swab, washed three times, and then photographed under a microscope with five randomly selected fields. The invasion assay involves diluting matrigel and spreading it on the upper chamber of the transwell chamber. After the gel solidifies, the remaining steps are the same as those in the migration experiment.

2.12 Mitochondrial Reactive Oxygen Species Detection

Two well-conditioned human NSCLC cell lines (shctrl and shFCRLB) were seeded in black-bottom, black-walled 96-well plates at a density of 1×10^5 cells/well and incubated overnight. Following a 1-hour incubation with a mitochondrial ROS fluorescent probe (Elabscience, E-BC-F008), fluorescence signal

intensity was measured using a microplate reader(Tecan) in top-read mode at excitation/emission (Ex/Em) wavelengths of 510/610 nm, with the signal intensity of the blank control group (containing probe only) subtracted for normalization.

2.13 Quantification of CCL2 Protein Concentration

Cell supernatants were collected from two NSCLC cell lines transfected with shCtrl or shFCRLB as experimental samples. CCL2 levels were quantified using a CCL2 ELISA kit (absin, abs510026). For detection, 100 μL of each sample or standard was added to the microplate wells and incubated for 2 hours. After washing, the primary antibody was added and incubated for another 2 hours. Subsequently, horseradish peroxidase (HRP) conjugate, chromogenic substrate, and stop solution (provided in the kit) were added sequentially. Absorbance was measured at 450 nm using a microplate reader (Tecan). CCL2 concentrations in the samples were calculated based on the standard curve, which was derived from the linear relationship between standard concentrations and their corresponding absorbance values.

2.14 assessment of FCRLB-Mediated Macrophage Polarization In Vitro

Six-week-old healthy male C57BL/6 mice were intraperitoneally injected with thioglycolate broth (Merck, 70157) for 4 consecutive days, then sacrificed after 4 days of reaction. Inject cold PBS into the abdominal cavity with a syringe, aspirate the liquid, filter through a 70 μm cell sieve (Yeasen, 84702ES50), centrifuge, and resuspend with red blood cell lysis buffer (Beyotime, C3702). After lysis, centrifuge to collect cells. Plate LLC cells (shCtrl and shFCRLB) at appropriate density, culture for 24 hours to collect supernatant, filter through a 0.22 μm membrane, and add to adherent mouse macrophages for 24-hour co-culture. Incubate the treated macrophages with CD86(Elabscience, E-AB-F0994D) and CD206(Elabscience, E-AB-F1135E) antibodies in the dark for 15 minutes, then detect cell polarization by flow cytometry.

2.15 Statistical Analysis

All graphs were generated using GraphPad Prism (10.1.2). Statistical analyses of intergroup differences were performed using Student’s t-test, one-way analysis of variance (one-way ANOVA), and two-way analysis of variance (two-way ANOVA). Differences were considered statistically significant at $p < 0.05$.

Table 1
Oligonucleotides used in this research

Nucleic acid type	Nucleic acid sequence
Human shRNA	
Scrambled control	TTCTCCGAACGTGTCACGTAA
FCRLB-1#	CCGCAAGCATTCTCTTTGAAT
FCRLB-2#	GCGAATTTCTTTCAAAGCCAT
Mouse shRNA	
FCRLB	GCTACTCTGGAGAAGCCTATA
Human primer	
18s sense	CAGCCACCCGAGATTGAGCA
18s anti-sense	TAGTAGCGACGGGCGGTGTG
FCRLB sense	AGTGGGCAAGCTGCTACTC
FCRLB anti-sense	CCGCTCCCCTTTGAAGATGG
Mouse primer	
ACTIN sense	GTGACGTTGACATCCGTAAAGA
ACTIN anti-sense	GCCGGACTCATCGTACTCC
FCRLB sense	ACCACCATCTTCAAGGGAGAG
FCRLB anti-sense	TACCAGAGAGTGCTAATGGGC

3. Results

3.1 Transcriptome data analysis of NSCLC

Through differentially analysis of LUAD, lung squamous cell carcinoma (LUSC) data and GSE101929, we identified 5895 downregulated genes and 6034 upregulated genes (Fig S1B) in the LUAD data, respectively; 7843 downregulated genes and 7957 upregulated genes (Fig S1C) in the LUSC data; and 2526 downregulated genes and 2444 upregulated genes in the GSE101929 dataset (Fig. 1A). GO and KEGG enrichment of up-regulated genes revealed BP pathways such as chromosome segregation, DNA templated DNA replication, and DNA replication, The chromosome region, condensed chromosome and other CC pathways, as well as single stranded DNA helicase activity, catalytic activity, acting on DNA and other MF pathways, were significantly enriched (Fig. 1B), while the Biosynthesis of cofactors, one carbon pool by folate and carbon metabolism pathways were significantly enriched (Fig. 1C). Subsequently, we

conducted RF gene screening and Cox regression analysis on LUAD and LUSC using co upregulated genes (Fig. 1D-G), and identified 12 genes that significantly affect the overall prognosis of lung cancer.

3.2 Single-cell analysis of NSCLC

To further analyze the mechanism of the selected key genes, we used single-cell data GSE131907. We first conducted single-cell analysis on a total of 208506 cells (Fig. 2A&Fig S2A-C), calculated all cell markers (Fig. 2B), and extracted single-cell data from tumor samples for subsequent analysis. We also performed expression localization analysis on twelve key genes (Fig. 2C). The results showed that SLC7A5, IER5L, ALDOA, FERMT1, and FCRLB genes were relatively highly expressed, but SLC7A5(16), IER5L(17), ALDOA(18), FERMT1(19) genes were studied more extensively, while the mechanism of FCRLB gene in lung cancer was less studied. Therefore, we chose FCRLB gene as the key gene for subsequent analysis. Through genetic mapping analysis, we found that the FCRLB gene is highly expressed in ts2 tumor cells and m0 Mac. Subsequently, we used the EMT gene set to score all tumor cells (Fig. 2D-E), and found that the EMT gene was highly expressed in ts2 and tumor ECs cells, indicating a higher degree of malignancy in ts2 cells.

3.3 Single-cell pseudo-temporal analysis

To further characterize ts2 cells, we first performed single-cell pseudo temporal analysis (Fig. 3A). Through analysis, it was found that ts2 is a mature differentiated cell, concentrated in the late stage of development. Ts2 is a mature differentiated cancer cell with specific functions. And through time-series gene analysis, we identified key genes that are highly expressed during ts2 differentiation (Fig. 3B-C), such as A1BG, ACAP3, AAMDC, etc. Subsequently, in order to further analyze the function of ts2 cells, we used single-cell gene set analysis (Fig. 3D) and found that ts2 cells highly expressed the reactive oxygen species pathway. After analyzing the key genes of the reactive oxygen species pathway (Fig. 3E), PRDX4 and ATOX1 genes were identified as key genes in the pathway. Subsequently, we used UCell, AUCell, ssgsea, and Singscore for analysis and found that ts2 cells were highly expressed in the reactive oxygen species pathway among the four algorithm scores (Fig. 3F-I). Subsequently, we used GSVA scoring to evaluate the Hallmark gene of MSIGDB on TS2 cells and FCRLB + TS2 cells (Fig. 3J-K). We found that both ts2 and FCRLB + ts2 overexpress the PI3K-AKT-MTOR signaling pathway. At the same time, we also conducted KEGG pathway analysis on FCRLB + ts2 (Fig. 3L), and found that FCRLB + ts2 overexpresses key tumor related pathways such as TGF-BETA and Apoptosis.

3.4 Cell Communication Analysis

To analyze the overall role of FCRLB in cancer regulation, we selected tumor cells and cancer cells for cell communication analysis (Fig. 4A-D). Through pathway analysis and receptor pairing analysis, we found that ts2 can specifically affect mo-Mac through VEGF, which is consistent with the results of gene set analysis, promoting M2-like macrophage polarization and further deteriorating the tumor microenvironment (Fig. 4E).

3.5 Single-cell metabolic analysis

In order to further elucidate the role of the FCRLB gene in the malignant progression of cancer cells, we divided the FCRLB gene expression into FCRLB + ts2 cells and FCRLB-ts2 cells, and performed single-cell metabolic analysis on these two cells (Fig. 5A). The results showed that the metabolic pathways of pyridine metabolism and Ubquinone and other terpenoid quinone biosynthesis were significantly upregulated (Fig. 5B). After analyzing the metabolomics of lung cancer blood samples and tissue samples, we found that the metabolic pathways of pyridine metabolism and Ubquinone and other terpenoid quinone biosynthesis were also significantly enriched (Fig. 5B). And at the same time, we selected key metabolites of the pyramididine metabolism and Ubquinone and other terpenoid quinone biosynthesis metabolic pathways from metabolomics data (Fig. 5C-D, F).

3.6 mo-Mac subgroup analysis

Subsequently, we conducted a detailed analysis of another key localization cell-mo-Mac. We first analyzed the immune cell microenvironment of single-cell normal samples and tumor samples, and found that the infiltration rate of mo-Macs significantly increased in lung cancer (Fig. 6A-B). Subsequently, we conducted gene set analysis on three types of Macs (Fig. 6C-D) and found that mo Macs highly expressed the Hedgehog pathway. Through key gene analysis of the Hedgehog pathway, we identified the VEGF gene as the pathway key gene (Fig. 6E). At the same time, we used FCRLB expression to group mo-Macs (Fig. 6F), and then performed GSVA analysis on FCRLB + mo-Macs and mo Macs (Fig. 6G-H). The results showed that mo-Macs overexpressed pathways such as inflammatory response and hypoxia, while FCRLB + mo-Macs overexpressed the reactive oxygen species pathway and PI3K-AKT-MTOR signaling pathway. According to the previous study(20), Mac can achieve M2 canopy polarization through the Hedgehog pathway. We used the M2 marker for localization and found (Fig. 6I) that the co localization result of CD163 and CD206 genes was mo-Mac, which is consistent with our hypothesis. Pseudo-temporal analysis revealed that mo-Macs are likely undergoing a dynamic process of differentiation or functional remodeling (Fig. 6J).

3.7 Validation that the FCRLB gene promotes malignant progression of NSCLC

To confirm the role of FCRLB in promoting the malignant progression of NSCLC, we utilized shRNA-mediated knockdown to downregulate FCRLB expression in these two cell lines and verified the knockdown efficiency (Fig. 7A-B). Knockdown of FCRLB can also significantly inhibit the growth rate of tumor cells (Fig. 7C-D). We further investigated the role of FCRLB in promoting metastasis and invasion; consistent with our predictions, the metastatic and invasive capacities of NSCLC cell lines were significantly impaired following FCRLB knockdown (Fig. 7E-H). We further verified the function of fcrlb in NSCLC. Mitochondrial reactive oxygen species levels were significantly reduced following FCRLB knockdown (Fig. 8A). Further quantification of CCL2 protein levels in cell supernatants demonstrated

that FCRLB can stimulate CCL2 production (Fig. 8B), while FCRLB knockdown decreased the activation of the PI3K-Akt signaling pathway upstream of CCL2 (Fig. 8C-D). Results from macrophage polarization assays demonstrated that FCRLB knockdown suppressed M2 polarization (Fig. 8E). We established a mouse subcutaneous tumor model using FCRLB-knockdown LLC1 cells (Fig. 9A). Compared with the shctrl group, FCRLB knockdown significantly reduced tumor volume and weight (Fig. 9B-D). IHC staining (Fig. 9E) of tumor samples demonstrated increased infiltration of M2-like macrophages and elevated CCL2 expression levels in the presence of FCRLB.

4. Discussion

Tumor-infiltrating macrophages, despite their phagocytic capacity to clear tumor cells, are predominantly polarized into pro-tumor M2 cells. These cells extensively secrete immunosuppressive factors (like IL-10, (21, 22)) and angiogenesis factors (like VEGF, MMP2) while highly expressing immune checkpoints such as PD-L1. They are widely recognized as core contributors to tumor progression and immune suppression, severely hindering the efficacy of immunotherapy and accelerating tumor growth. Therefore, reducing macrophage recruitment and M2 polarization is considered key to eliminating the adverse effects associated with TAMs(21–23). Interestingly, previous studies have demonstrated that tumors can remodel the tumor microenvironment by secreting metabolites. These metabolites modulate macrophage polarization toward the M2 subtype via the Hedgehog signaling pathway, thereby promoting malignant proliferation(24, 25). Through identification, it has been demonstrated that metabolites modulate the chemotaxis and infiltration of TAMs by regulating the expression of multiple cytokines, including CCL2, in tumor cells(26). The Hedgehog signaling pathway is recognized as a critical driver of tumor progression across diverse tumor models and is linked to enhanced macrophage infiltration and polarization(24, 27, 28). Tumor-derived CCL2 serves to recruit macrophages and promote M2 polarization, with activation of the Hedgehog signaling pathway in TAMs exerting a critical role in this process(29, 30).

In this study, we found that FCRLB gene was highly expressed in ts2 tumor cells, and EMT gene set score showed that ts2 cells were highly malignant. Signaling pathway enrichment analysis revealed that mo-Mac cells exhibit upregulation of the Hedgehog signaling pathway. Analyses of FCRLB-positive and FCRLB-negative subgroups yielded results similar to those from the ts2 analysis. CCL2, a downstream effector molecule of the PI3K signaling pathway(31), effectively activate the Hedgehog signaling pathway to induce macrophage M2-polarization, as noted previously. Furthermore, results from cell-cell communication analyses support specific CCL2-mediated crosstalk between ts2 and mo-Mac cell populations. To obtain a more comprehensive understanding of the malignant functions of FCRLB, metabolic analyses of FCRLB-positive and FCRLB-negative populations revealed significant upregulation of pyrimidine metabolism as well as ubiquinone and other terpenoid-quinone biosynthesis pathways, with key metabolites identified. Results from HPLC further demonstrated changes in these metabolites following FCRLB overexpression and knockout.

FCRLB, a newly identified member of the Fc receptor-like family, was initially believed to exert an immunomodulatory role(32, 33). Previous studies have demonstrated that FCRLB plays a critical role in the inhibitory pathway of B cell signaling and can effectively suppress key downstream signaling pathways in B cells(34). Some studies have demonstrated that FCRLB serve as a favorable prognostic factor in chronic lymphocytic leukemia and regulate immune activation processes during malignant progression(35, 36). However, research on this gene remains limited; its specific functions, involved signaling networks, and regulatory roles in solid tumors are still poorly understood. Herein, through the integration of multi-omics and machine learning, advanced transcriptome analyses, and validation in cellular models, animal models, and clinical samples, we have, for the first time, comprehensively investigated the characteristics of FCRLB in promoting malignant progression in NSCLC and elucidated its regulatory role in tumor-macrophage crosstalk. This not only broadens our understanding of the signaling networks underlying tumor remodeling of the TME but also identifies highly promising therapeutic targets.

Our work also has some limitations. Firstly, although we have discovered the pro-tumor regulatory role of FCRLB in NSCLC, the specific signaling mechanism is still unclear, and its natural ligand is still unknown. Further research on FCRLB monoclonal antibodies and epigenetics is needed to investigate the association between malignant pathways and FCRLB. Secondly, although CCL2 has been found to play an important role in the ts2-mo-Mac signaling interaction in our cell communication research and has received significant attention as a recognized macrophage infiltration factor, other FCRLB mediated cytokines also require comprehensive research. Multi factor testing may provide us with stronger support in subsequent research. Then, further exploration is needed to identify small molecule targeted drugs for FCRLB, including screening small molecule drug libraries, screening suitable small molecule compounds, and verifying their functions in animal models, which can better demonstrate the clinical potential of this target.

5. Conclusion

We screened the key gene FCRLB that affects the prognosis of lung cancer through transcriptome gene screening, and analyzed the unique role of FCRLB in tumor cells and macrophages. Tumor cells with high expression of FCRLB showed high activation of PI3K and reactive oxygen pathways, regulating pyridine metabolism and other terpenoid quinone biosynthesis pathways, inducing CCL2 expression. Also, high FCRLB expression in mo-Mac, promote M2-like polarization, and further exacerbate the malignancy of lung cancer.

Abbreviations

FCRLB
Fc receptor-like B
NSCLC
non-small cell lung cancer

ROS
reactive oxygen species
CCL2
C-C motif chemokine ligand 2
TME
tumor microenvironment
TAMs
tumor-associated macrophages
mo-Macs
monocyte-derived macrophages
LUAD
lung adenocarcinoma
WB
Western blot
CCK8
Cell Counting Kit-8
one-way ANOVA
one-way analysis of variance
two-way ANOVA
two-way analysis of variance
LUSC
lung squamous cell carcinoma

Declarations

Ethics approval and consent to participate

The animal study was reviewed and approved by the Animal Experiment Ethics Committee of Zhejiang University before implementation (ZJU20250631).

Consent for publication

Consent to publish was obtained from the study participants.

Availability of data and materials

The datasets used and/or analysed during the current study are available from the corresponding author on reasonable request.

Competing interests

The authors declare that they have no competing interests.

Funding

This work was funded by the National Natural Science Foundation of China (No. 82203608 to X.Z.Y. and No. 32300753 to S.Y.L.), Huadong Medicine Joint Funds of the Zhejiang Provincial Natural Science Foundation of China (LHDMY23H160002 to X.Z.Y.).

Author contribution

Nueraili Maihemuti, Yueli Shi, Sujing Jiang, Pan Liu, Zhen Shi and Zhiyong Xu designed the study, performed experiments, analyzed data, and wrote the manuscript. Nueraili Maihemuti, Yueli Shi and Sujing Jiang performed experiments and analyzed data. Zhiyong Xu, Zhen Shi and Pan Liu conceived and designed the study and wrote the manuscript.

Acknowledgements

The authors acknowledge the data provided by databases including TCGA and GEO. Appreciation is expressed to the reviewers and editors for their constructive comments.

References

1. Siegel RL, Kratzer TB, Giaquinto AN, Sung H, Jemal A. Cancer statistics, 2025. CA Cancer J Clin. 2025;75(1):10-45.
2. Meyer ML, Fitzgerald BG, Paz-Ares L, Cappuzzo F, Jänne PA, Peters S, et al. New promises and challenges in the treatment of advanced non-small-cell lung cancer. Lancet. 2024;404(10454):803-22.
3. Liu M, Hu S, Yan N, Popowski KD, Cheng K. Inhalable extracellular vesicle delivery of IL-12 mRNA to treat lung cancer and promote systemic immunity. Nat Nanotechnol. 2024;19(4):565-75.
4. Lahiri A, Maji A, Potdar PD, Singh N, Parikh P, Bisht B, et al. Lung cancer immunotherapy: progress, pitfalls, and promises. Mol Cancer. 2023;22(1):40.
5. Li Y, Yan B, He S. Advances and challenges in the treatment of lung cancer. Biomed Pharmacother. 2023;169:115891.
6. Tang H, You T, Ge H, Bai C, Wang Y, Sun Z, et al. Autophagy inhibition improves the efficacy of anlotinib and PD-1 inhibitors in the treatment of NSCLC. J Immunother Cancer. 2025;13(9).
7. Goudot C, Coillard A, Villani AC, Gueguen P, Cros A, Sarkizova S, et al. Aryl Hydrocarbon Receptor Controls Monocyte Differentiation into Dendritic Cells versus Macrophages. Immunity. 2017;47(3):582-96.e6.
8. Hu H, Li X, Xu Z, Tao Y, Zhao L, You H, et al. OPG promotes lung metastasis by reducing CXCL10 production of monocyte-derived macrophages and decreasing NK cell recruitment. EBioMedicine. 2025;111:105503.
9. Park MD, Reyes-Torres I, LeBerichel J, Hamon P, LaMarche NM, Hegde S, et al. TREM2 macrophages drive NK cell paucity and dysfunction in lung cancer. Nat Immunol. 2023;24(5):792-801.

10. Han S, Wang W, Wang S, Yang T, Zhang G, Wang D, et al. Tumor microenvironment remodeling and tumor therapy based on M2-like tumor associated macrophage-targeting nano-complexes. Theranostics. 2021;11(6):2892-916.
11. Liu L, Chen G, Gong S, Huang R, Fan C. Targeting tumor-associated macrophage: an adjuvant strategy for lung cancer therapy. Front Immunol. 2023;14:1274547.
12. Zhang H, Mu Q, Jiang Y, Zhao X, Jia X, Wang K, et al. Integrative single-cell and machine learning approach to characterize immunogenic cell death and tumor microenvironment in LUAD. J Transl Med. 2025;23(1):1000.
13. Wang Y, Zhang L, Xie H, Wang L, Wang Y, Li S, et al. Predicting response and survival of lung adenocarcinoma under anti-programmed death-1 therapy using biological deep learning. Brief Bioinform. 2025;26(5).
14. Xie J, Zhao S, Wu D, Ma C, Yan W, Zhang P, et al. A Metabolism-Driven Prognostic Model and PSMD14-SP1-GYS1 Axis Reveal Therapeutic Vulnerabilities in Melanoma. J Invest Dermatol. 2025.
15. Qian X, Zhang HY, Li QL, Ma GJ, Chen Z, Ji XM, et al. Integrated microbiome, metabolome, and proteome analysis identifies a novel interplay among commensal bacteria, metabolites and candidate targets in non-small cell lung cancer. Clin Transl Med. 2022;12(6):e947.
16. Liu Y, Ma G, Liu J, Zheng H, Huang G, Song Q, et al. SLC7A5 is a lung adenocarcinoma-specific prognostic biomarker and participates in forming immunosuppressive tumor microenvironment. Heliyon. 2022;8(10):e10866.
17. Chen X, He YQ, Miao TW, Yin J, Liu J, Zeng HP, et al. IER5L is a Prognostic Biomarker in Pan-Cancer Analysis and Correlates with Immune Infiltration and Immune Molecules in Non-Small Cell Lung Cancer. Int J Gen Med. 2023;16:5889-908.
18. Chang YC, Chan YC, Chang WM, Lin YF, Yang CJ, Su CY, et al. Feedback regulation of ALDOA activates the HIF-1α/MMP9 axis to promote lung cancer progression. Cancer Lett. 2017;403:28-36.
19. Liu B, Feng Y, Xie N, Yang Y, Yang D. FERMT1 promotes cell migration and invasion in non-small cell lung cancer via regulating PKP3-mediated activation of p38 MAPK signaling. BMC Cancer. 2024;24(1):58.
20. Hinshaw DC, Hanna A, Lama-Sherpa T, Metge B, Kammerud SC, Benavides GA, et al. Hedgehog Signaling Regulates Metabolism and Polarization of Mammary Tumor-Associated Macrophages. Cancer Res. 2021;81(21):5425-37.
21. Zhang Y, Zheng H, Zhang R, Li J, Yang S, Hua Y, et al. Pancreatic cancer cells escape T/NK cell immune surveillance through the expressional separation of CD58. J Immunother Cancer. 2025;13(9).
22. Lin T, Hou Y, Liu X, Ullah I, Qiu S, Lu Z, et al. Fluorinated Proteolysis Targeting Chimeras-Sorafenib Nanoassembly for Epigenetic Remodeling to Combat Multi-Pathway Drug Resistance in Hepatocellular Carcinoma. ACS Nano. 2025.
23. Duan X, Hu K, Wang J, Wang X, Long X, Lin W, et al. Core-shell engineered Col/Cs@ECM microspheres for macrophage-targeted intracellular drug release in RA therapy. Bioact Mater.

2025;54:715-29.

24. Petty AJ, Li A, Wang X, Dai R, Heyman B, Hsu D, et al. Hedgehog signaling promotes tumor-associated macrophage polarization to suppress intratumoral CD8+ T cell recruitment. J Clin Invest. 2019;129(12):5151-62.
25. Chen D, Zhang X, Li Z, Zhu B. Metabolic regulatory crosstalk between tumor microenvironment and tumor-associated macrophages. Theranostics. 2021;11(3):1016-30.
26. Chen J, Sun HW, Wang RZ, Zhang YF, Li WJ, Wang YK, et al. Glutamate promotes CCL2 expression to recruit tumor-associated macrophages by restraining EZH2-mediated histone methylation in hepatocellular carcinoma. Oncoimmunology. 2025;14(1):2497172.
27. Zhu HZ, Zhou WJ, Wan YF, Ge K, Lu J, Jia CK. Downregulation of orosomucoid 2 acts as a prognostic factor associated with cancer-promoting pathways in liver cancer. World J Gastroenterol. 2020;26(8):804-17.
28. Zhu L, Yang Y, Li H, Xu L, You H, Liu Y, et al. Exosomal microRNAs induce tumor-associated macrophages via PPARγ during tumor progression in SHH medulloblastoma. Cancer Lett. 2022;535:215630.
29. Guo X, Zhang H, He C, Qin K, Lai Q, Fang Y, et al. RUNX1 promotes angiogenesis in colorectal cancer by regulating the crosstalk between tumor cells and tumor associated macrophages. Biomark Res. 2024;12(1):29.
30. Cascio S, Chandler C, Zhang L, Sinno S, Gao B, Onkar S, et al. Cancer-associated MSC drive tumor immune exclusion and resistance to immunotherapy, which can be overcome by Hedgehog inhibition. Sci Adv. 2021;7(46):eabi5790.
31. Boutet M, Nishitani K, Couturier N, Erler P, Zhang Z, Militello AM, et al. Mutations in MLL3 promote breast cancer progression via HIF1α-dependent intratumoral recruitment and differentiation of regulatory T cells. Immunity. 2025;58(8):2035-53.e9.
32. Davis RS, Wang YH, Kubagawa H, Cooper MD. Identification of a family of Fc receptor homologs with preferential B cell expression. Proc Natl Acad Sci U S A. 2001;98(17):9772-7.
33. Owen CJ, Kelly H, Eden JA, Merriman ME, Pearce SH, Merriman TR. Analysis of the Fc receptor-like-3 (FCRL3) locus in Caucasians with autoimmune disorders suggests a complex pattern of disease association. J Clin Endocrinol Metab. 2007;92(3):1106-11.
34. Shabani M, Bayat AA, Jeddi-Tehrani M, Rabbani H, Hojjat-Farsangi M, Ulivieri C, et al. Ligation of human Fc receptor like-2 by monoclonal antibodies down-regulates B-cell receptor-mediated signalling. Immunology. 2014;143(3):341-53.
35. Li FJ, Ding S, Pan J, Shakhmatov MA, Kashentseva E, Wu J, et al. FCRL2 expression predicts IGHV mutation status and clinical progression in chronic lymphocytic leukemia. Blood. 2008;112(1):179-87.
36. Shea LK, Honjo K, Redden DT, Tabengwa E, Li R, Li FJ, et al. Fc receptor-like 2 (FCRL2) is a novel marker of low-risk CLL and refines prognostication based on IGHV mutation status. Blood Cancer J. 2019;9(6):47.

Figures

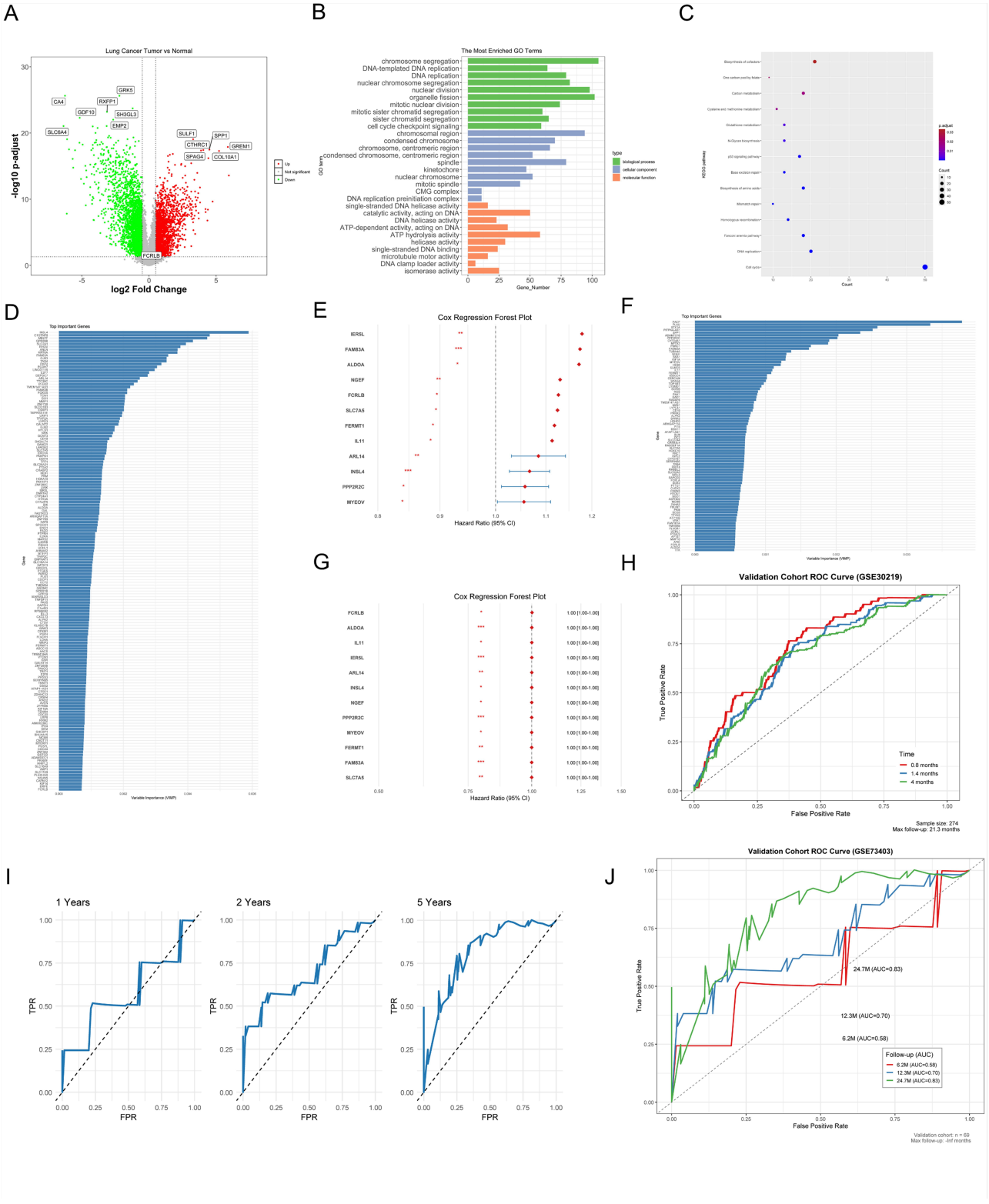


Figure 1

Identification of common upregulated genes and their clinical relevance in lung adenocarcinoma (LUAD) and lung squamous cell carcinoma (LUSC).

(A) Volcano plot illustrating differentially expressed genes (DEGs) from GSE dataset analysis. Red dots denote upregulated genes, blue dots denote downregulated genes, and gray dots denote genes with no significant difference ($|\log_2$fold change (FC)$| > 1$, adjusted $P < 0.05$).(B) Gene Ontology (GO) enrichment analysis of common upregulated genes, showing significantly enriched biological processes, cellular components, or molecular functions.(C) Kyoto Encyclopedia of Genes and Genomes (KEGG) pathway enrichment analysis of common upregulated genes, highlighting significantly enriched signaling pathways.(D) Random Forest (RF) feature importance scoring plot for common upregulated genes in the LUAD dataset, ranking genes by their importance in predicting clinical outcomes.(E) Forest plot of Cox proportional hazards regression analysis for common upregulated genes in LUAD, displaying hazard ratios (HRs) and 95% confidence intervals (CIs) to assess their prognostic significance.(F) RF feature importance scoring plot for common upregulated genes in the LUSC dataset, ranking genes by their importance in predicting clinical outcomes.(G) Forest plot of Cox proportional hazards regression analysis for common upregulated genes in LUSC, displaying HRs and 95% CIs to assess their prognostic significance.(H–J) Receiver operating characteristic (ROC) curves for validating the predictive performance of the gene signature in external datasets, with area under the curve (AUC) values indicated.

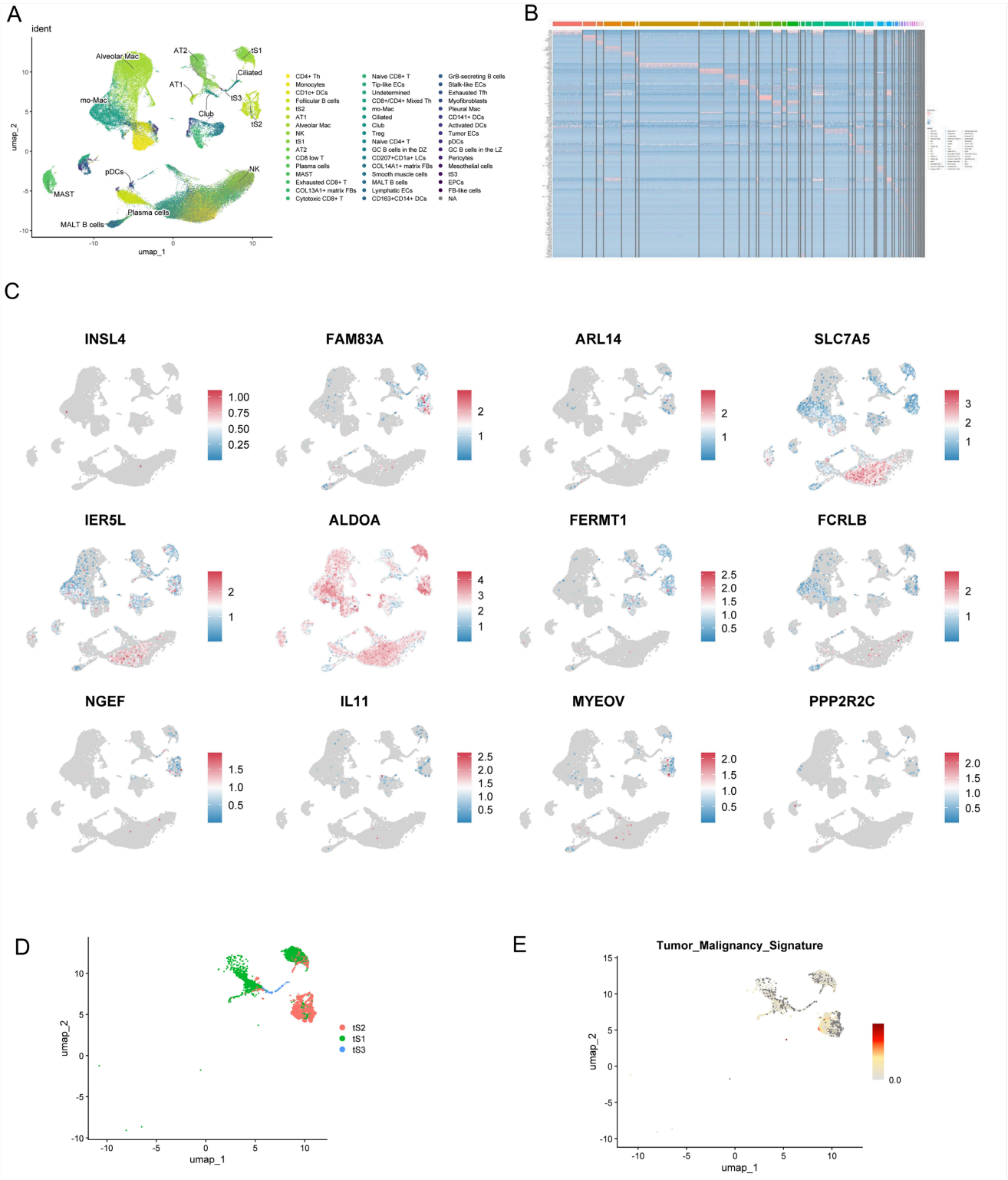


Figure 2

Single-cell transcriptomic characterization of lung cancer cells and analysis of key gene/EMT signature distribution.

(A) UMAP plot of dimensionality reduction for lung cancer single-cell RNA sequencing (scRNA-seq) data. (B) Heatmap of marker genes for lung cancer single-cell clusters. Rows represent cluster-specific marker

genes. (C) Single-cell localization feature plot of key genes in lung cancer. (D) UMAP plot of dimensionality reduction for tumor cells isolated from lung cancer scRNA-seq data. (E) UMAP plot of lung cancer tumor cells overlaid with EMT gene set enrichment scores.

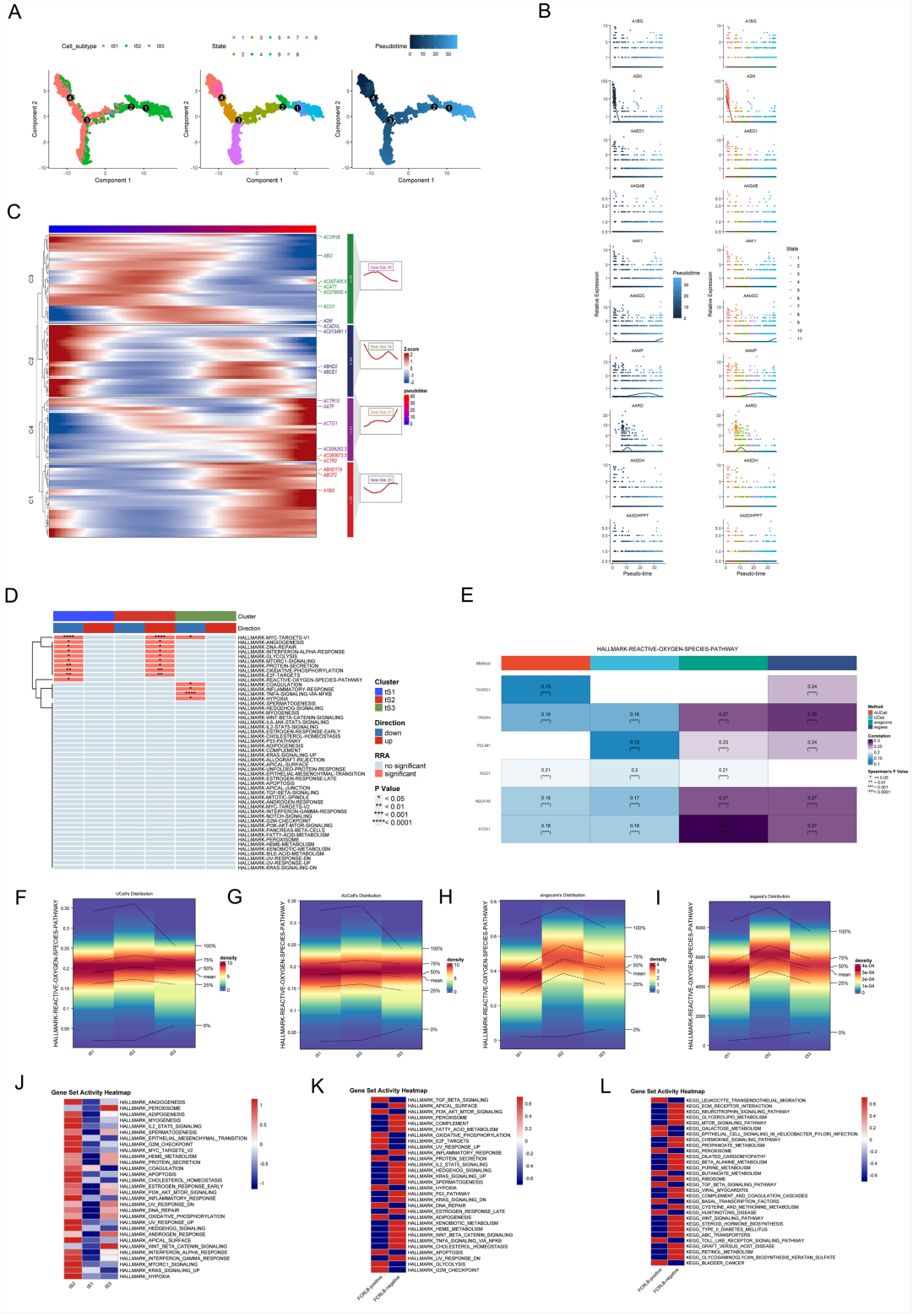


Figure 3

Pseudotime trajectory analysis and pathway enrichment scoring of lung cancer single cells.

(A) Single-cell pseudotime trajectory plot of lung cancer cells. (B) Temporal expression profiles of the top 10 differentially expressed genes (DEGs) along pseudotime. (C) Temporal heatmap of key genes and their co-expression modules along pseudotime. Rows represent either target key genes. (D) Hallmark gene set enrichment score plot along pseudotime. The x-axis denotes pseudotime.(E) Analysis plot of key genes in the reactive oxygen species (ROS) pathway.(F) UCell algorithm: x-axis = UCell score for the ROS pathway (higher scores = stronger pathway activation), y-axis = cell density. Colors distinguish (G) AUCell algorithm: Same structure as (F), with x-axis = AUCell score for the ROS pathway. (H) singscore algorithm: Same structure as (F), with x-axis = singscore score for the ROS pathway. (I) ssGSEA algorithm: Same structure as (F), with x-axis = ssGSEA score for the ROS pathway. (J–K) Heatmaps of Hallmark pathway enrichment scores calculated via GSVA. (L) Heatmap of KEGG pathway enrichment scores calculated via GSVA.

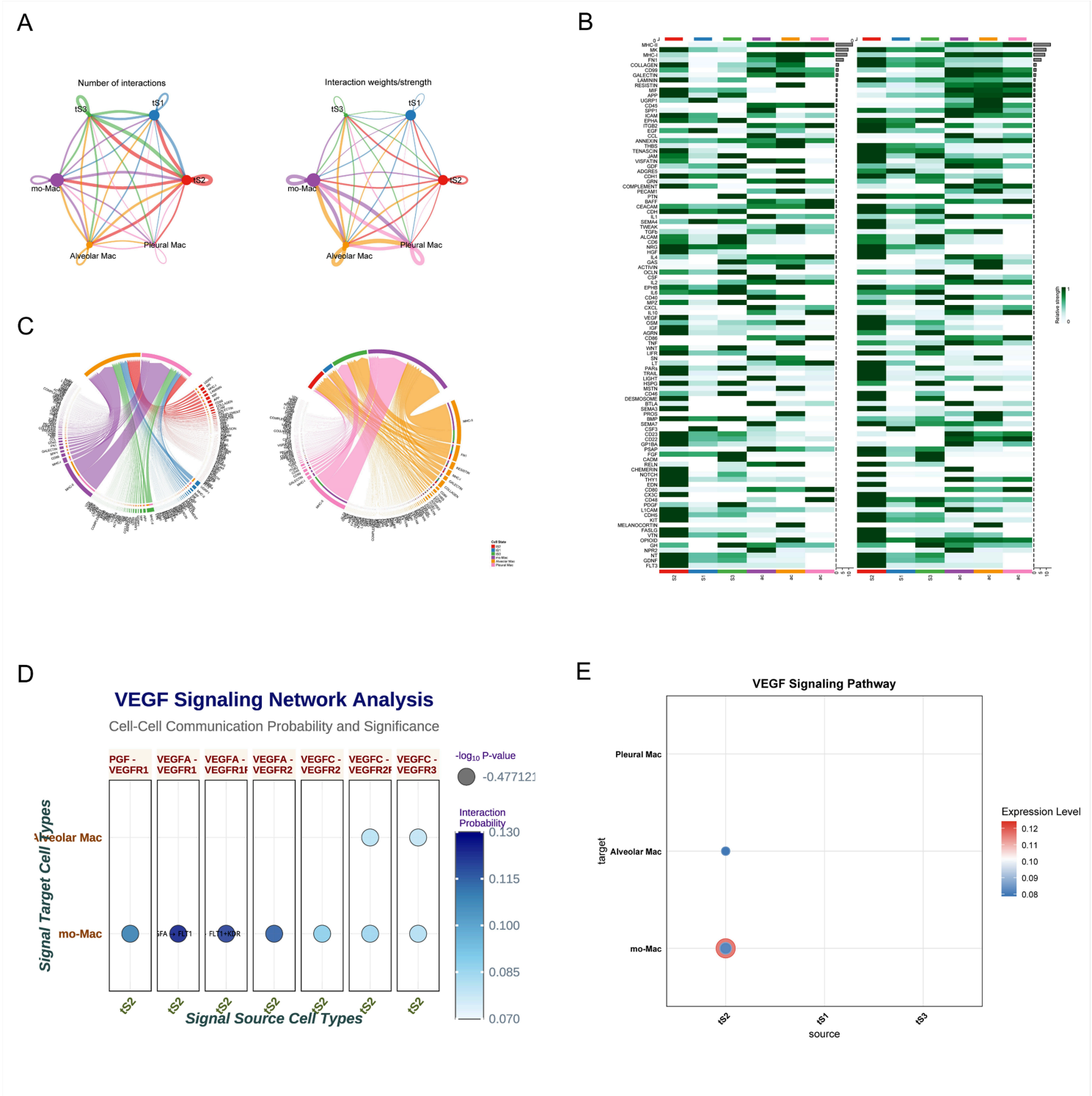


Figure 4

Cell-cell communication profiling in the lung cancer microenvironment using single-cell RNA sequencing (scRNA-seq) data.

(A) Quantification plot of cell-cell communication intensity and quantity. (B) Cell-cell communication pathway network plot. (C) Chord diagram of cell-cell communication. (D) VEGF signaling pathway communication intensity plot. (E) Ligand-receptor (L-R) pair analysis plot for the VEGF signaling pathway.

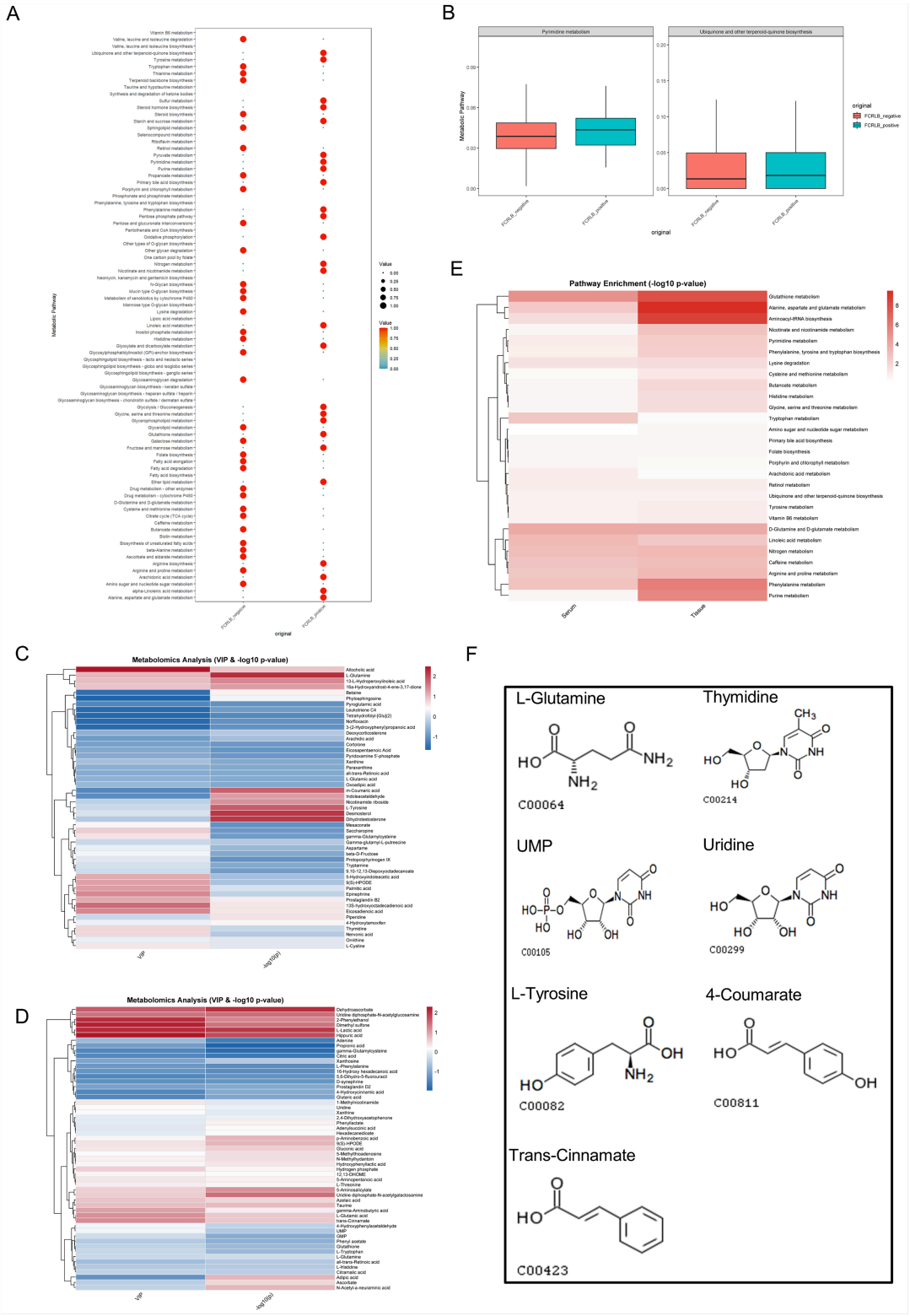


Figure 5

Metabolic characterization of lung cancer across single-cell, serum, and tissue samples.

(A) Dot plot for single-cell metabolic analysis of lung cancer cells. (B) Box plot for single-cell metabolic analysis of lung cancer cells. (C) Heatmap of key metabolites in serum samples from lung cancer patients vs. healthy controls. (D) Heatmap of key metabolites in lung cancer tissue samples vs. adjacent

normal tissue samples. (E) Heatmap of key metabolic pathways in lung cancer vs. normal samples. (F) Key metabolites.

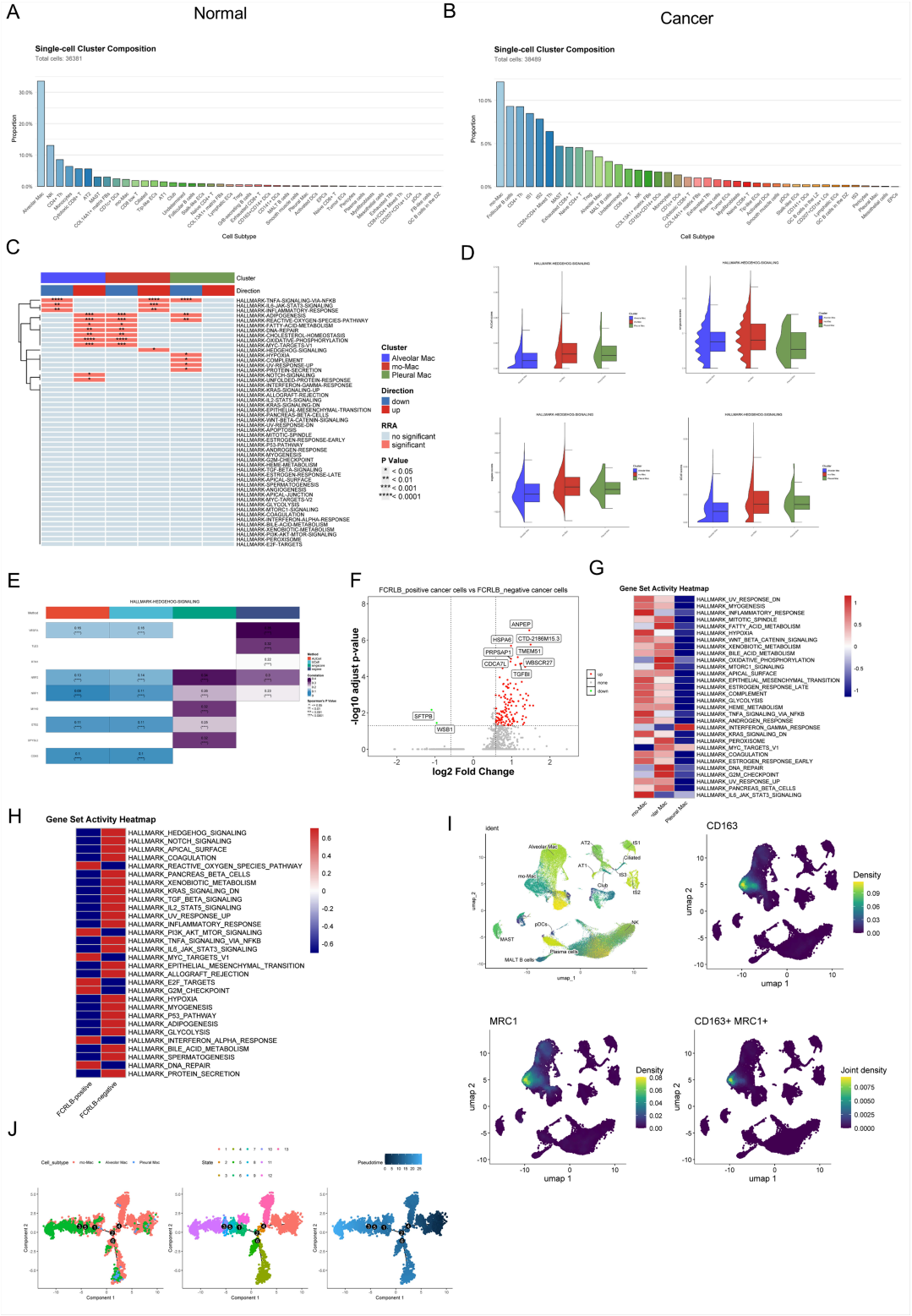


Figure 6

Single-cell characterization of immune cell subsets, IL-6-JAK-STAT pathway activity, and mo-Mac (monocyte-derived macrophage) dynamics in normal vs. lung cancer samples.

(A) Cell proportion plot of single-cell populations in normal samples. (B) Cell proportion plot of single-cell populations in lung cancer samples. (C) Analysis plot of macrophage (macrophage) gene sets. (D) Half-violin plot of IL-6-JAK-STAT pathway activity scored by four algorithms. (E) Key gene analysis plot of the IL-6-JAK-STAT pathway. (F) Volcano plot of differential gene expression between $FCRLB^{+}$ mo-Mac and $FCRLB^{-}$ mo-Mac subsets. (G) Heatmap of Hallmark pathway enrichment scores (via GSVA) across cell subsets/sample groups. (H) Heatmap of Hallmark pathway enrichment scores (via GSVA) specifically in mo-Mac cell. (I) Co-localization plot of CD163 and CD206 genes. (J) Single-cell pseudotime trajectory plot of macrophages.

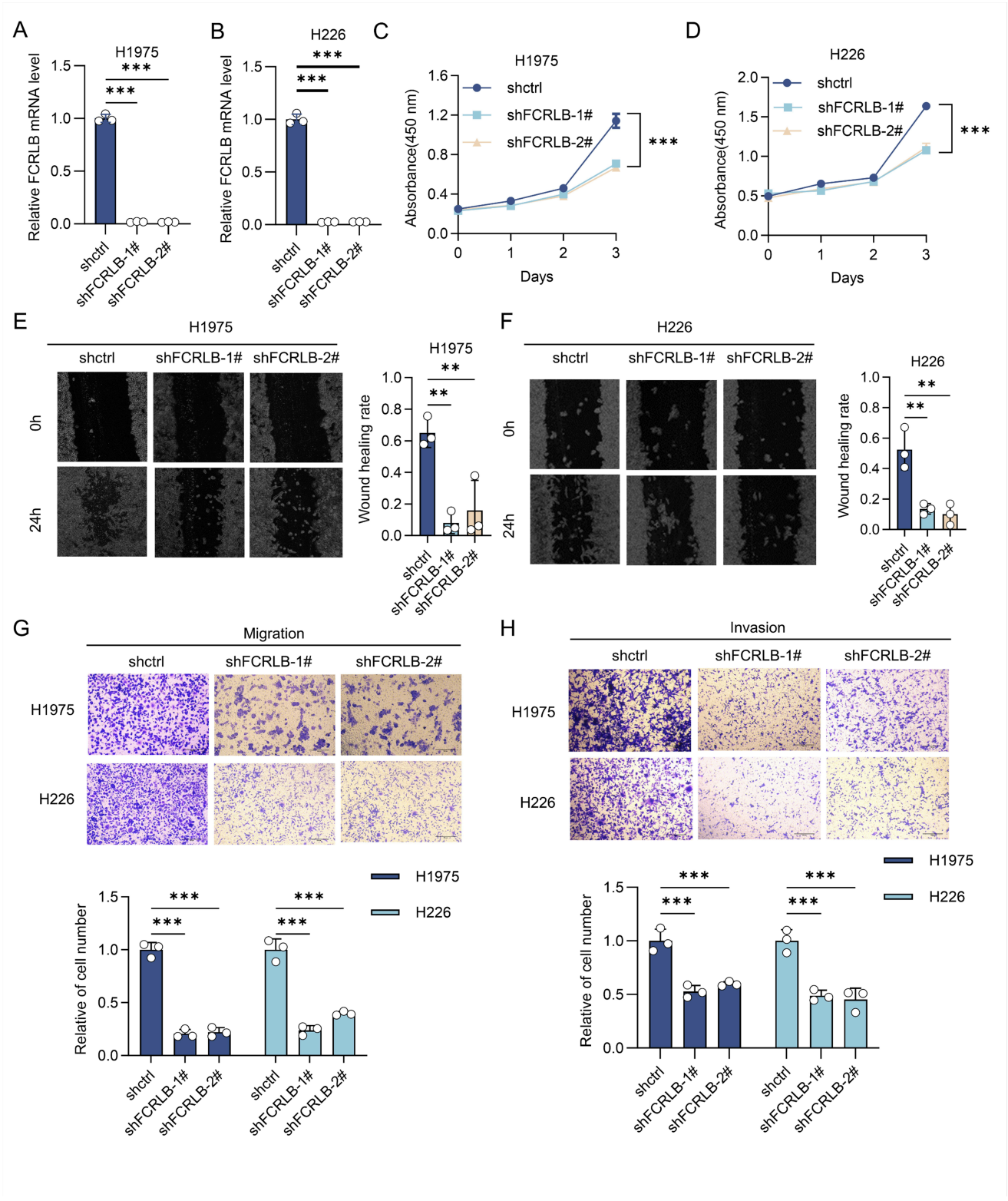


Figure 7

FCRLB knockdown impairs proliferation, migration, and invasion of lung cancer cells.

(A-B) Quantitative real-time PCR (qRT-PCR) analysis of FCRLB mRNA expression in H1975 and H226 cells transduced with control shRNA (shCtrl), or two independent FCRLB-targeting shRNAs (shFCRLB-1#, shFCRLB-2#). (C-D) Cell proliferation was assessed by CCK-8 assay in H1975 (C) and H226 (D) cells

transduced with shCtrl, shFCRLB-1#, or shFCRLB-2# over a 3-day time course. (E-F) Wound healing assays were performed in H1975 (E) and H226 (F) cells transduced with shCtrl, shFCRLB-1#, or shFCRLB-2#; representative images of wound areas at 0 h and 24 h (left panels) and quantification of wound closure rate (right panels) are shown.(G) Transwell migration assays of H1975 and H226 cells transduced with shCtrl, shFCRLB-1#, or shFCRLB-2#; representative crystal violet-stained images of migrated cells are shown.(H) Transwell invasion assays (using Matrigel-coated inserts) of H1975 and H226 cells transduced with shCtrl, shFCRLB-1#, or shFCRLB-2#; representative crystal violet-stained images of invaded cells (left panels) and quantification of invaded cell numbers (right panels) are shown***P ≤ 0.001, **P ≤ 0.002, *P ≤ 0.05.

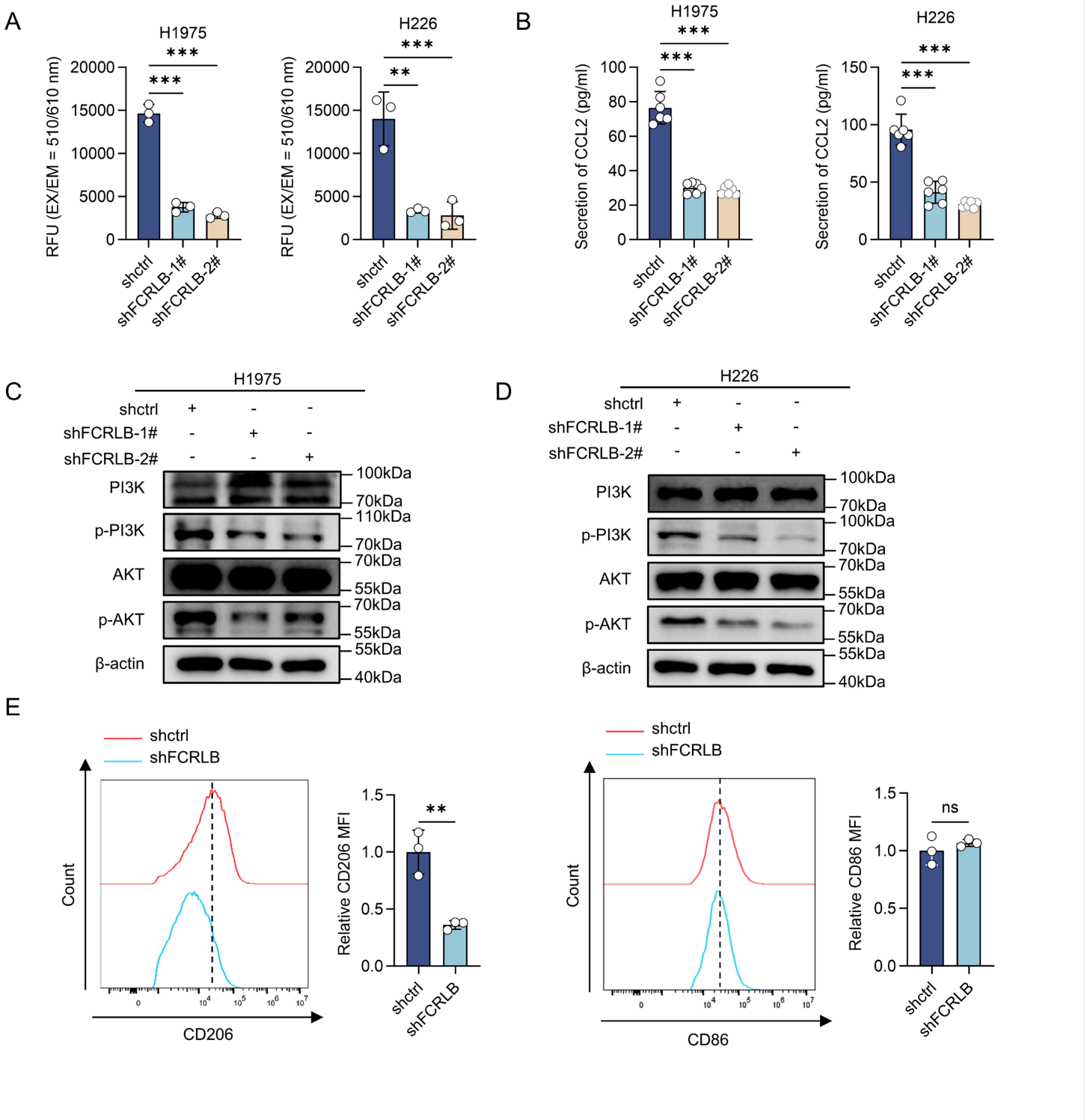


Figure 8

Effects of FCRLB knockdown on mitochondrial ROS levels, CCL2 secretion, PI3K-AKT pathway activation, and macrophage polarization in non-small cell lung cancer (NSCLC) cells.

(A) Mitochondrial reactive oxygen species (ROS) levels in two NSCLC cell lines transduced with control shRNA (shCtrl), shFCRLB-1#, or shFCRLB-2# were detected using a fluorescence microplate reader at an

excitation wavelength (Ex) of 510 nm and an emission wavelength (Em) of 610 nm. (B) ELISA was performed to measure the expression level of CCL2 in the cell supernatant of two NSCLC cell lines transduced with shCtrl, shFCRLB-1#, or shFCRLB-2#. (C–D) WB analysis was used to detect the protein levels of key components in the PI3K-AKT signaling pathway in two NSCLC cell lines transduced with shCtrl, shFCRLB-1#, or shFCRLB-2#. (E) Flow cytometry was employed to assess the effect of cell supernatant from LLC1 cells transduced with shCtrl or shFCRLB on the polarization of primary macrophages. ***P ≤ 0.001, **P ≤ 0.002, *P ≤ 0.05.

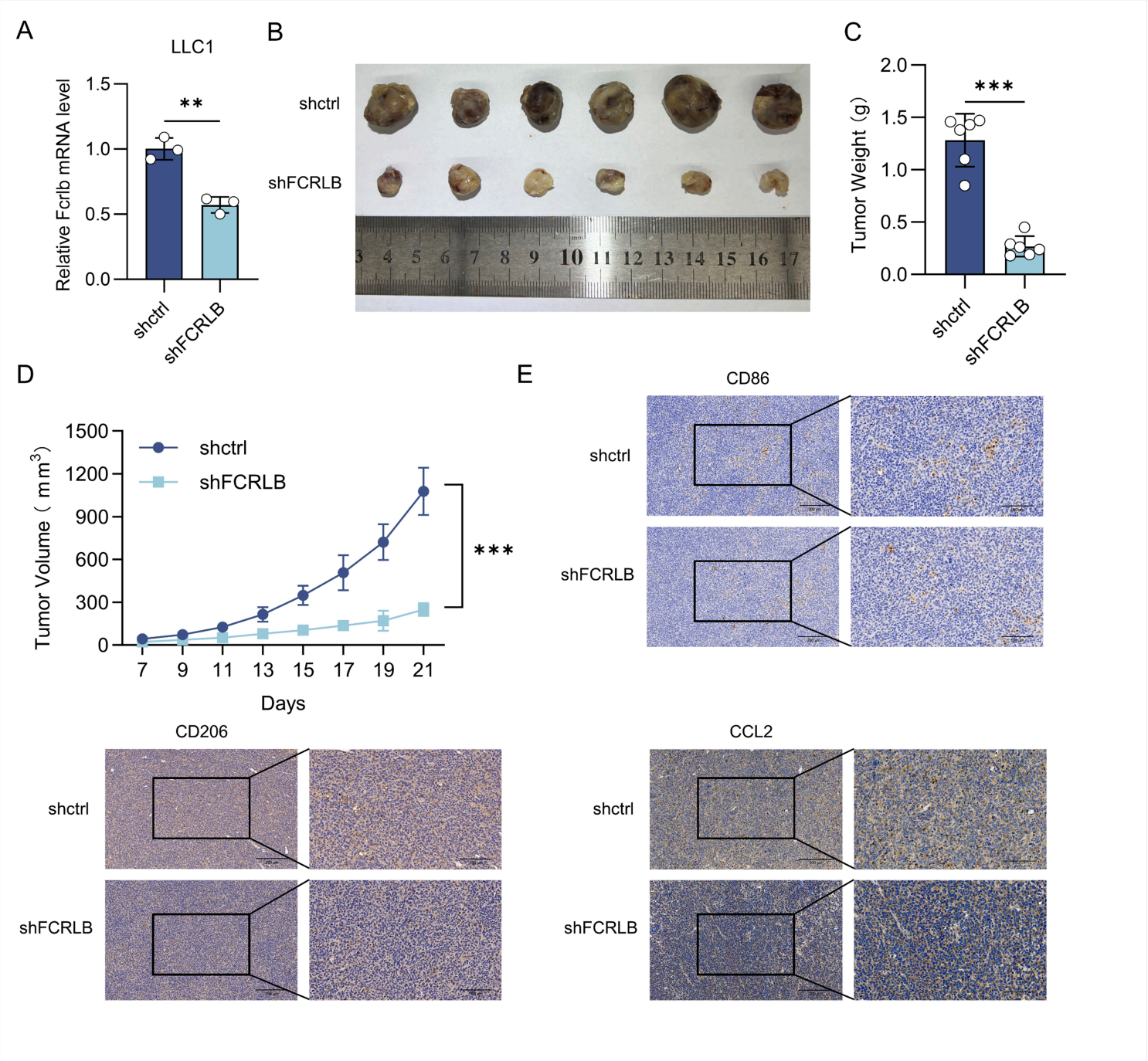


Figure 9

In vivo validation of FCRLB function in a murine LLC subcutaneous xenograft model.

(A) Quantitative real-time PCR (qRT-PCR) analysis of FCRLB knockdown efficiency in LLC cells. (B) Representative images of tumors isolated from C57BL/6 mice after subcutaneous xenograft of shctrl- or shFCRLB-transduced LLC cells. (C) Tumor weight comparison between shctrl and shFCRLB xenograft groups. (D) Tumor growth curves of shctrl and shFCRLB xenografts. (E) Immunohistochemical (IHC) staining results of CD86, CD206, and CCL2 in shCtrl and shFCRLB tumors. ***P ≤ 0.001, **P ≤ 0.002, *P ≤ 0.05.

Supplementary Files

This is a list of supplementary files associated with this preprint. Click to download.

- SupplementaryMaterial.pdf